

Geophysical Research Letters[®]

RESEARCH LETTER

10.1029/2022GL101472

Key Points:

- A reduction in October northern Baffin Bay ice cover is observed around 2001 and is characterized by a westward retreat of the ice edge
- The spatiotemporal shift in the ice cover coincided with observed warming of surface air and ocean temperatures to inhibit ice growth
- An ocean model suggests the ice loss is spatially coherent with Atlantic water mass warming on the eastern flank of northern Baffin Bay

Supporting Information:

Supporting Information may be found in the online version of this article.

Correspondence to:

T. J. Ballinger,
tjballinger@alaska.edu

Citation:

Ballinger, T. J., Moore, G. W. K., Garcia-Quintana, Y., Myers, P. G., Imrit, A. A., Topál, D., & Meier, W. N. (2022). Abrupt northern Baffin Bay autumn warming and sea-ice loss since the turn of the twenty-first century. *Geophysical Research Letters*, 49, e2022GL101472. <https://doi.org/10.1029/2022GL101472>

Received 28 SEP 2022

Accepted 24 OCT 2022

Author Contributions:





Conceptualization: Thomas J. Ballinger, G. W. K. Moore

Formal analysis: Thomas J. Ballinger, G. W. K. Moore, Yarisbel Garcia-Quintana, Amreen A. Imrit, Dániel Topál

Methodology: Thomas J. Ballinger, G. W. K. Moore, Dániel Topál

Writing – review & editing: Thomas J. Ballinger, G. W. K. Moore, Yarisbel Garcia-Quintana, Paul G. Myers, Amreen A. Imrit, Dániel Topál, Walter N. Meier

Abrupt Northern Baffin Bay Autumn Warming and Sea-Ice Loss Since the Turn of the Twenty-First Century

Thomas J. Ballinger¹ , G. W. K. Moore^{2,3} , Yarisbel Garcia-Quintana^{3,4} , Paul G. Myers⁴ , Amreen A. Imrit⁵, Dániel Topál^{6,7}, and Walter N. Meier⁸

¹International Arctic Research Center, University of Alaska Fairbanks, Fairbanks, AK, USA, ²Department of Physics, University of Toronto, Toronto, On, Canada, ³Department of Chemical and Physical Sciences, University of Toronto Mississauga, Toronto, On, Canada, ⁴Department of Earth and Atmospheric Sciences, University of Alberta, Edmonton, AB, Canada, ⁵Department of Mechanical Engineering, University of Toronto, Toronto, On, Canada, ⁶Institute for Geological and Geochemical Research, Research Centre for Astronomy and Earth Sciences, ELKH, MTA-Centre for Excellence, Budapest, Hungary, ⁷ELTE Eötvös Loránd University, Doctoral School of Environmental Sciences, Budapest, Hungary, ⁸National Snow and Ice Data Center, Cooperative Institute for Research in Environmental Sciences, University of Colorado, Boulder, CO, USA

Abstract A delay in autumn sea ice formation is an important consequence of Arctic Amplification. Baffin Bay is one such region impacted by delayed ice formation, though spatiotemporal analyses to date have not detailed the evolution and drivers of such autumn ice changes. In this study, we document abrupt Baffin Bay sea ice cover changes in the key transition month of October from 1950 to 2021. The ice cover mean and variance dramatically change from 2001 onward with a transition to largely ice-free conditions in the northeast and thinner ice in the northwest. Ocean model experiments attribute these changes to warming of the Atlantic-origin water (AOW) flowing into northeastern Baffin Bay from the south. Transport and upwelling of this above-freezing AOW has stunted ice formation in this area, while the basin's cyclonic surface current has contributed to reduced cooling and ice formation in the northwestern portion of Baffin Bay.

Plain Language Summary Delayed sea ice formation during autumn is a signature of Arctic warming, which affects regional Arctic climates and ecosystems. Baffin Bay is one such area of later ice growth through time, which we investigate further with observations and an ocean model. Our analyses show a remarkable change in Baffin Bay's ice cover since 2001. In the last two decades (2001–2021), northeastern Baffin Bay has transitioned from partially ice-covered to a primarily open-water state with ice formation now occurring ~2 weeks later. Observations suggest much warmer surface temperatures are responsible for this change in the ocean environment. An ocean modeling experiment confirms this recent ice loss pattern and attributes it to the transport of warm Atlantic water across northern Baffin Bay.

1. Introduction

A robust signature of Arctic Amplification is the lengthening of the sea ice melt season (Stroeve & Notz, 2018). Pervasive across the Arctic, this expansion is the product of shoulder, or “transition,” season ice losses associated with earlier spring (March – May) ice break-up and melt and later autumn (September – November) ice formation and advance. Baffin Bay is one Arctic marginal sea characterized by notable shoulder season ice cover changes. Basin-wide observations have revealed large autumn sea-ice extent reductions (Onarheim et al., 2018) coinciding with delayed freeze onset (Ballinger et al., 2018). Around Baffin Island, Moore (2006) found the largest ice reductions during the shoulder seasons with autumn losses on the order of 20% in Cumberland Sound and 10%–15% for western Davis Strait from 1979 to 2004. Spatial trends of Baffin Bay autumn sea ice concentration (SIC) from 1979 to 2015 indicated autumn total SIC decline on the order of ~20%–30% along the northwest Greenland coastline region, encompassing the eastern portion of the North Water region (Stroeve et al., 2017).

Changes to Baffin Bay's ice conditions play a key role in the region's biological and physical environment. Northern Baffin Bay, including areas of shorefast ice cover, has shown sensitivity to warming with impacts on the local marine ecosystem and the communities that live around its coastline (Cooley et al., 2020; Meier et al., 2006). This region is also home to the largest and most productive Arctic polynya, the North Water (Ingram et al., 2002). This feature is critically dependent on the formation of ice arches along Nares Strait that block the transport of thick multi-year Arctic sea ice in northern Baffin Bay (Barber et al., 2001). There is evidence that

the flux of multi-year ice along Nares Strait is increasing while the stability of the arches is decreasing (Moore et al., 2021). Warming of Baffin Bay waters also have implications on the Greenland Ice Sheet (GrIS). Decreased sea ice and mélange has been associated with the retreat and melt of northwest Greenland's outlet glaciers (Moon et al., 2015; Wood et al., 2021), while GrIS meltwater runoff has been linked to enhanced heat content in Baffin Bay (Castro de la Guardia et al., 2015). Atmospheric responses and feedbacks due to Baffin Bay's warming and ice loss have also been identified, including intensification of katabatic winds (Heinemann, 2003) and synoptic anticyclones aloft (Sellevold et al., 2022).

Given the region's physical and biological sensitivity to warming, we expand upon past analyses by revisiting northern Baffin Bay autumn season ice cover variability and change characteristics. We direct focus on October as a key time of change within the transition season as Baffin Bay ice cover commonly formed during this month in the 1980s and 1990s, but more recently in situ ice formation has tended to occur later in the autumn season (Ballinger et al., 2018). Our goal is to identify when and where the predominantly first-year October ice cover in Baffin Bay has changed, and understand the role of near-surface and upper-ocean thermodynamics in facilitating these changes. To this end, we evaluate Baffin Bay ice cover for temporal changes, then analyze such changes against local/regional weather station and reanalysis-derived surface air and ocean temperatures, and use a high-resolution ocean model, NEMO, to evaluate how oceanic characteristics and processes within Baffin Bay have influenced its ice conditions through time.

2. Data and Methods

Variability and spatial patterns of October northern Baffin Bay ice variables (i.e., sea ice area (SIA) and SIC) are analyzed from multiple sources. We examine SIA from ERA5 (Hersbach et al., 2020) and SIBT1850 (Walsh et al., 2019) since 1950. Before the passive microwave satellite era, sea ice charts and reports are common between these products as described in Titchner and Rayner (2014) and Walsh et al. (2019). The NOAA/NSIDC Climate Data Record (CDR) of SIC (Meier et al., 2021, 2022) is used for analyses since 1979. Additional descriptions and comparisons of these SIA products are provided in Text S1 and Figure S1 of Supporting Information S1. Unless otherwise stated, SIC is measured along a centerline transect extending 400 km (75°N) south of Smith Sound, which marks the southern boundary of the North Water (Dunbar, 1969).

Multiple temperature parameters are analyzed to understand thermodynamic contributions to northern Baffin Bay's ice variability. Two-meter air (T_{2m}) and skin temperatures (T_{skin}) for ocean grid cells within northern Baffin Bay (74–78°N and 55–85°W), where most early freeze season ice is present, are also obtained from ERA5 reanalysis. ERA5 T_{skin} data are comprised of SST over the open ocean and surface ice temperature over sea ice. T_{2m} observations from the terrestrial automatic weather station at Kitsissut (04203), located in northern Baffin Bay (76.63°N, 73.00°W; 11m asl), are used to supplement the ERA5 temperature fields (Cappelen, 2021). From the T_{2m} data, we derive freezing degree days (FDDs), which are simply calculated as the daily mean T_{2m} departure from freezing summed across all October days. Over the ocean, we apply an additional FDD constraint of SIC $\geq 15\%$ to include only the freezing temperatures that contributed to sea ice production.

To isolate oceanographic features and forcing associated with Baffin Bay's observed ice changes, we examine SIC, SST, sea ice thickness and production, and sea-surface salinity, depth-averaged temperature of Atlantic-origin Water (AOW), and heat content at the bottom of the mixed layer from a Nucleus for European Modeling of the Ocean (NEMO; Madec et al., 2008) v3.6 model run. The physical ocean model was configured for the Arctic and North Atlantic (ANHA4 configuration, simulation EPM111 with explicit tidal forcing), and coupled to the Louvain-la-neuve ice module (version 2; Vancoppenolle et al., 2009). The ANHA4 domain, described in Hu et al. (2018) and Castro de la Guardia et al. (2019), provides five-day output of physical and hydrographic fields across the sampling region over with a 0.25° horizontal resolution and vertical discretization in 50 depth bins (1 m resolution at surface, increasing non-linearly to >100 m at depth). The simulation was run over 1970–2021, forced by atmospheric data from the CORE Reanalysis (1970–2009; Large & Yeager, 2008), extended through 2021 with NCEP/NCAR fields (Kalnay et al., 1996), river and glacier freshwater input from Stadnyk et al. (2020) and Bamber et al. (2018), and tidal data from TOPEX/Poseidon Global Inverse Solution TPXO 8 (Egbert & Erofeeva, 2002). The AOW is defined here as a water mass with temperature $\geq 0^\circ\text{C}$ and salinity >33.8 psu.

Baffin Bay ice cover has been shown to vary and change on sub-decadal to multidecadal timescales (Grumet et al., 2001; Stern & Heide-Jørgensen, 2003). To objectively test for statistically significant Baffin Bay October

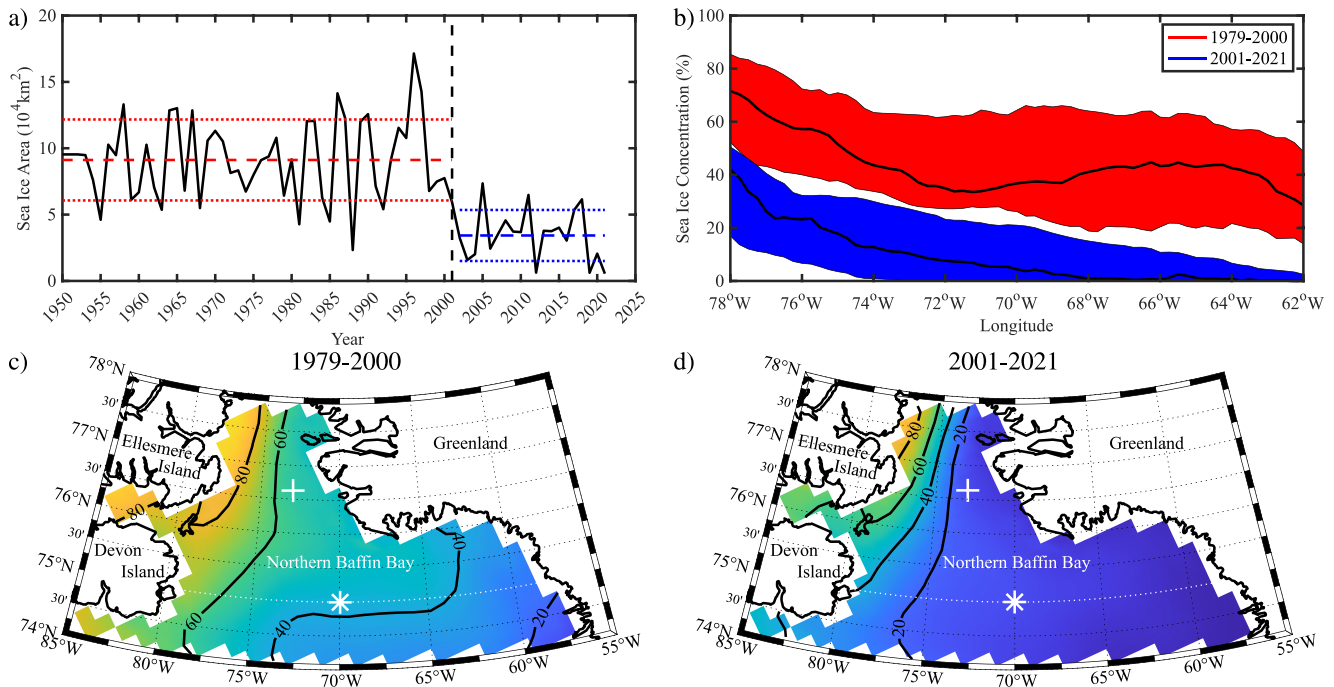


Figure 1. Spatial and temporal variability in northern Baffin Bay sea ice. (a) Sea ice area (SIA; 10^4 km^2) time series from ERA5, 1950–2021. A Pettitt test is used to identify the statistically significant SIA distribution change that occurred in 2001. Means before and after this breakpoint are indicated by the red and blue dotted lines. The standard deviation for the two periods are indicated by the thick dotted white lines in (c) and (d), for the periods 1979–2000 and 2001–2021. The black curves are the medians for the two periods with the shading representing the variability bounded by the respective 1st and 3rd quartiles. Spatial variability in the mean SIC from the CDR product across 75°N , indicated by the thick dotted white lines in (c) and (d), for the periods 1979–2000 and 2001–2021. The black curves are the medians for the two periods with the shading representing the variability bounded by the respective 1st and 3rd quartiles. Spatial variability in the mean SIC from the CDR product for: (c) 1979–2000, and (d) 2001–2021 with the asterisk symbol indicating the location within the North Water where results are shown in subsequent figures, and the plus sign indicating the location of the Kitsissut weather station.

SIA mean and variance changes within the SIA time series, we apply the non-parametric Pettitt change point technique (Pettitt, 1979). These breaks informed averaging periods for subsequent plots and analyses. Recognizing the non-Gaussian distribution of sea ice and temperature, we track median, first and third quartile changes of these parameters by longitude. Hovmöller diagrams are additionally used to examine northern Baffin Bay inter-annual T_{skin} and FDD changes as a function of longitude.

3. Results

3.1. Spatiotemporal Changes in Baffin Bay Ice Cover

Baffin Bay-wide October SIA anomaly time series from ERA5 are shown in Figure 1a. After applying the Pettitt test, a SIA changepoint is identified in 2001. Of note, a break in 2001 is also found in the passive-microwave constrained CDR product and in 1998 in the SIBT1850 product (Figure S1 in Supporting Information S1). This abrupt break in the ERA5 SIA time series is reflected in distribution changes from 1950 to 2000 to 2001–2021 as the mean is reduced by more than a factor of two ($9.2 \times 10^4 \text{ km}^2$ versus $3.6 \times 10^4 \text{ km}^2$), and the variance decreased by $\sim 36\%$ ($3.1 \times 10^4 \text{ km}^2$ versus $2.0 \times 10^4 \text{ km}^2$). Since 1979, both ERA5 and CDR show good agreement ($r > 0.99$) and similar variability before and after 2001, though $\sim 1000 \text{ km}^2$ more ice is found in the CDR in both periods likely due to its lower resolution. Given relative distribution similarities, we elect to focus our remaining Baffin Bay analyses on the satellite era, including use of the CDR product.

During October, most of the first-year Baffin Bay ice cover that forms and advances does so from its northernmost area. To showcase these changes, we track longitudinal SIC variability along 75°N (Figure 1b). With respect to the 2001 breakpoint, distinct variability and cross-basin SIC reductions are apparent between periods. From 1979 to 2000, median Baffin Bay SIC ranged from $\sim 30\%$ in northeast ($\sim 62^\circ\text{W}$) to $\sim 70\%$ in the northwest ($\sim 78^\circ\text{W}$). Another telling SIC change is that the overall variability (shaded area between the quartiles) decreased from the former to latter period especially in northeasternmost Baffin Bay ($62\text{--}72^\circ\text{W}$). Spatial changes

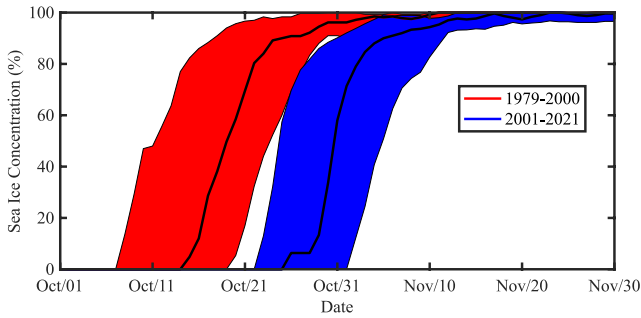


Figure 2. Temporal variability in sea ice conditions at 75°N and 70°W during October and November, 1979–2021. The black curves are the medians for the two periods with the shading representing the variability bounded by the respective 1st and 3rd quartiles. All data are from the CDR product.

between the two periods are also striking (Figures 1c and 1d). Compared to 1979–2000 (Figure 1c), there is notable westward ice retreat and constriction of the SIC gradient from 2001 to 2021 (Figure 1d). For example, the 20% SIC contour, an ice edge approximation, is barely visible ~60–62.5°W in 1979–2000. However, the same contour dramatically shifts westward to ~75°W in 2001–2021, yielding, on average, a much broader fetch of open water conditions.

In the North Water region of Baffin Bay (75°N, 70°W) where we previously noted a shift from ice-covered to ice-free conditions, we take a closer look at daily October SIC variability as a function of time. From 1979 to 2000, median ice cover in the North Water began to form late in the second week of the month, reaching ~80% concentration by October 21 (Figure 2). Ice formation in the second half of the record tended to form roughly two weeks later, growing to 80% ice coverage by early November.

We further investigate the progression of recent daily SIC changes during autumn (Figure S2 in Supporting Information S1). Within the North Water, the daily SIC is shown, with upper-and-lower bound shading marking the third and first quartiles over the period 1979–2021. There is considerable interannual variability in the daily ice cover including years such as 1987, 1996, and 1997 where ice growth occurred earlier than climatology as well as years such as 2002, 2006 and 2019 where ice growth was delayed. Consistent with the results shown in Figure 2, ice growth in the 1979–2000 period occurred earlier than in the more recent period.

3.2. Observed Thermodynamic Forcing of Baffin Bay's Ice Changes

In the absence of substantial ice cover in preceding melt season months, we posit reduced northern Baffin Bay SIC stems from thermodynamic changes. To test this hypothesis, we track the temporal evolution of surface temperatures across northern Baffin Bay by analyzing ERA5 T_{skin} and FDDs when sea ice was present (Figure 3). Moving east-to-west across the basin at 75°N, it is apparent that around the identified 2001 breakpoint that T_{skin} warming in excess of the salinity-adjusted freezing point (Figure 3a) clearly emerged in tandem with reduced

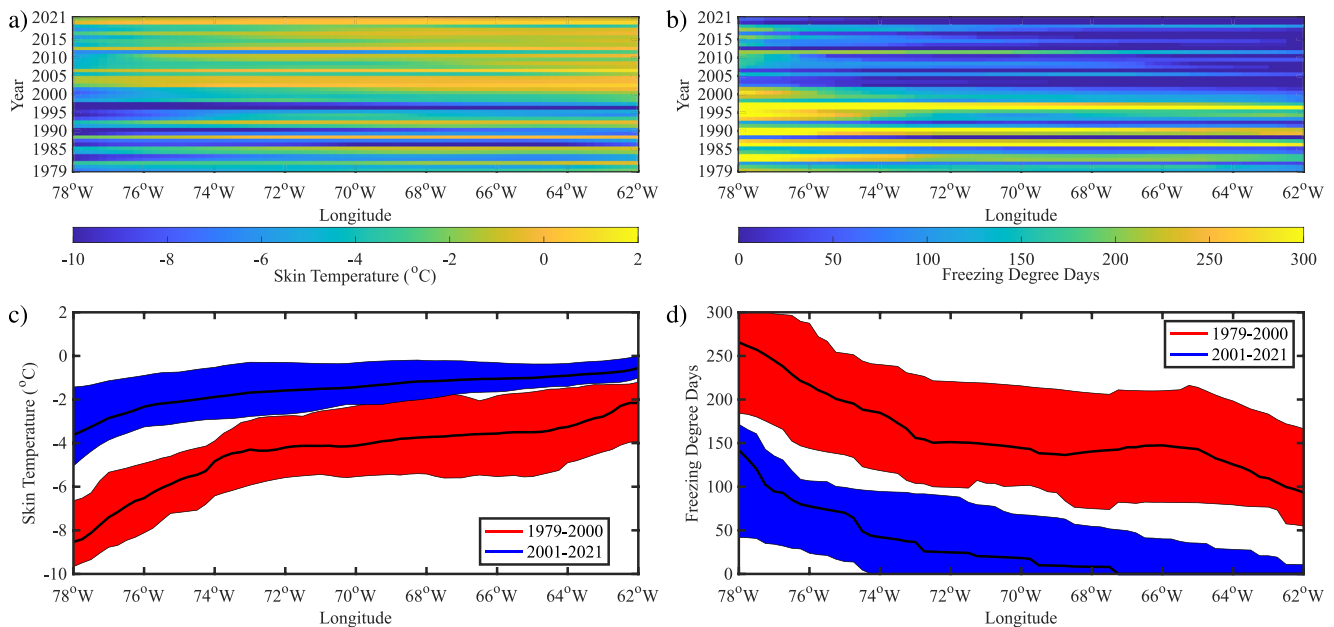


Figure 3. Variability in surface conditions during October along 75°N. Hovmöller diagrams are shown for: (a) skin temperature (T_{skin} ; °C) and (b) freezing degree days (FDDs) when sea ice is present. The median and variance for the period 1979–2000 and 2001–2021 for T_{skin} is shown in (c) and FDDs in (d). The black curves signify the median for these periods and the shading represents the variability as represented by the 1st and 3rd quartiles. All data are from ERA5.

FDDs over sea ice (Figure 3b) and at the Kitsissut weather station (Figure S3 in Supporting Information S1). In some Octobers, for example ~2004 and 2005, a cross-basin (62–78°W) melt signature occurred with <50 cumulative FDDs.

In terms of variability, less ice cover in northeastern versus northwestern Baffin Bay (Figure 1b) is associated with more consistently warm warmer waters on the easternmost area (Figure 3c). Recent surface temperature warming has also coincided with contracted temperature variability (blue shaded area), especially in the easternmost longitudes. Above-freezing T_{skin} temperatures at 75°N stretched across easternmost Baffin Bay (62–70°W), suggesting even “colder” years today are warmer than “warm” years pre-2000. The T_{skin} median from 2001 to 2021 also shows a rather gentle horizontal temperature gradient to 74–78°W where temperatures drop in the vicinity of known downwelling (Melling et al., 2001), but not to magnitudes seen in previous decades. Figure 3d shows that FDDs followed the T_{skin} changes through time. Whereas modest variability in freezing temperatures occurred in northeastern Baffin Bay from 1979 to 2000 (~50–150 FDDs at 62°W), median FDDs in 2001–2021 only emerged around ~67°W with “cold” years since 2001 exhibiting relatively minimal freeze conditions (<50 FDDs) to ~66°W aligned with surface warming and ice loss.

3.3. Insights on Baffin Bay Warming and Melt From an Ocean Model Experiment

We analyze the NEMO model run in an attempt to better understand oceanic contributions to the observed surface temperature and attendant sea ice changes. Relative to the satellite-derived SIC observations (Figure 1b), NEMO generally captures the spatial patterns of SIC across northern Baffin Bay at 75°N (Figure 4a). For example, during 1979–2000, October median SIC ranges from ~20 to 40% across ~62–71°W, followed by a marked SIC increase from ~40 to 80% moving westward from 74 to 78°W. Reduced ice cover variability in NEMO versus the CDR is apparent when comparing the two time periods in both products, and this discrepancy may result from differences in spatial resolution amongst other factors. Despite some differences, the general SIC spatial pattern (i.e., lower (higher) SIC in the east (west)) and changes with respect to time are maintained, yielding confidence in NEMO to resolve sea ice thickness and production patterns (Figures 4b and 4c) and associated physical controls across the basin.

We further utilize NEMO to understand surface and upper-ocean conditions attributed to sea ice variability (Figure 5). From 1979 to 2000, SSTs in northeastern Baffin Bay (~55–65°W near the Greenland coast) are $\geq -1^\circ\text{C}$, and transition to cooler temperatures and increased ice production moving westward across the basin (Figure 5a). The 2001–2021 mean SSTs are comparatively much warmer with the -1°C contour shifting $\sim 10^\circ$ westward to ~75°W (Figure 5d). More striking are that near to above-freezing temperatures permeated northeastern Baffin Bay (~55–65°W), including a warm tongue (0.5°C) within this region around ~74–75°N. AOW warming above the freezing point expanded westward as shown by an increase in shaded grid cells extending to ~75–80°W. Along the Greenland coast, the AOW has warmed by roughly a factor of two between 1979 and 2000 (Figure 5b) and 2001–2021 (Figure 5e) with the largest warming proximate to the aforementioned SST warm tongue. Furthermore, the heat content over the mixed layer depth has also substantially increased through time (Figures 5c and 5f). As mixing tends to occur ~40 m depth in northern Baffin Bay, where strong warming ($\sim 2\text{--}6 \times 10^6 \text{ J}$) is noted (Figures 5c and 5f), the upward mixing of this heat can have a negative impact on sea-ice growth.

4. Summary, Discussion, and Conclusions

Dramatic October ice cover changes in Baffin Bay transpired around 2001. Since that time, reductions in the SIC mean (>200%) and variance (~36%) relative to 1979–2000 occurred as open water engulfed much of northeasternmost Baffin Bay. In northwestern Baffin Bay, an area of historically thicker, more developed October ice cover, a notable decrease in SIC also occurred. We show that the timing of ice formation has also shifted across northern Baffin Bay by ~2 weeks from the middle of October to month's end since 2001. These ice regime changes were accompanied by surface warming in excess of the freezing point with fewer sub-freezing episodes as suggested by concurrent FDD declines. Regarding the oceanographic setting, in the absence of spatially coherent changes in salinity, which would signal changes in ocean currents flowing into and circulating within northern Baffin Bay (Figure S4 in Supporting Information S1), a NEMO run suggests that the depth-averaged AOW has warmed and its mixing has entrained oceanic heat into the surface to drive the region's ice loss since 2001.

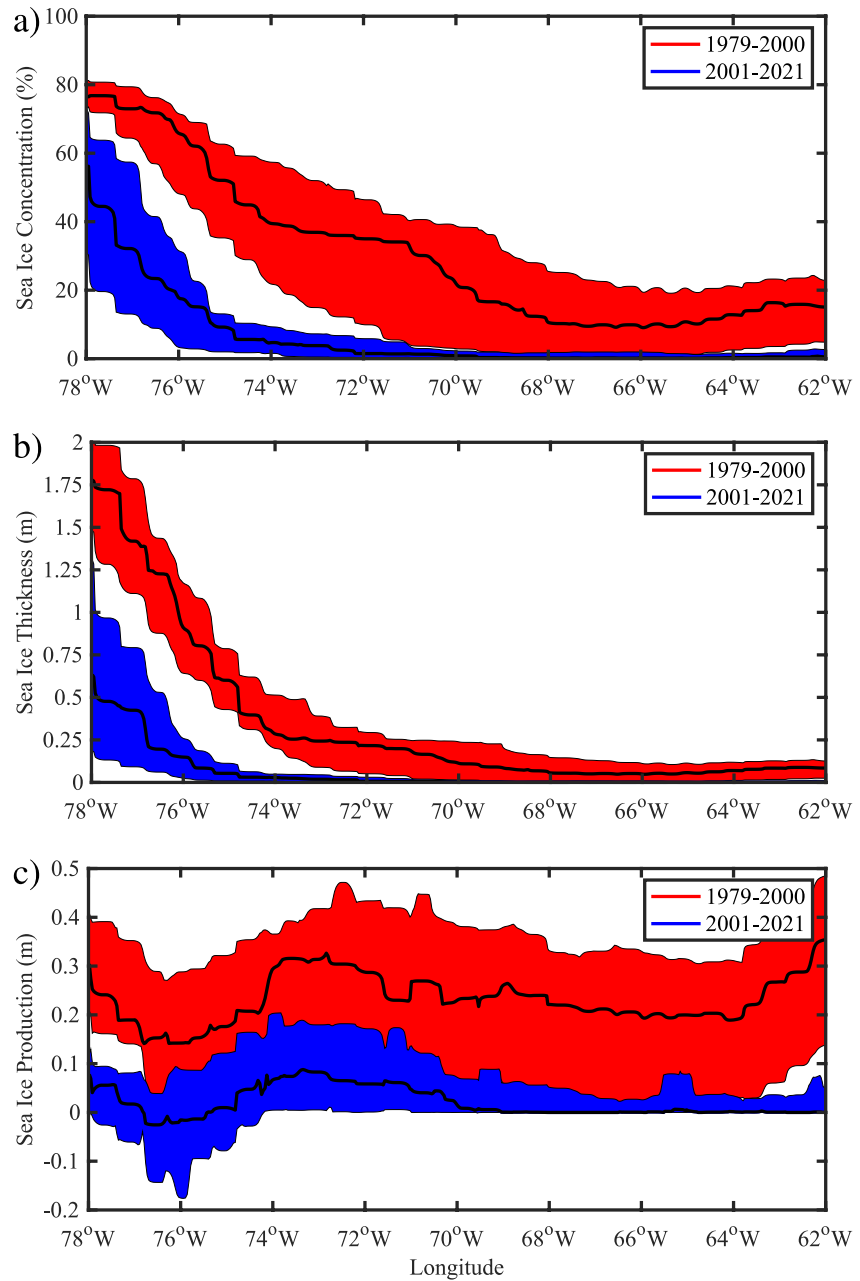


Figure 4. Variability in sea ice characteristics during October along 75°N. The 1979–2000 and 2001–2021 median and variance are presented for: (a) SIC (%), (b) sea ice thickness (m), and (c) sea ice production (m). The black curves show the median for these periods, and the shading represents the variability as indicated by the 1st and 3rd quartiles. All data are from the NEMO model run.

As part of the International North Water Project, Melling et al. (2001) observed and documented the ocean circulation and hydrography in northern Baffin Bay, noting that poleward flow in the West Greenland Current (WGC) tends to diverge at the Greenland coast, supporting upwelling and entrainment of the warm AOW to the ocean surface. As the WGC transports the AOW water poleward, near Smith Sound/southern Nares Strait (~78°N) the prevailing flow curves southward in tandem with downwelling of surface waters. This re-direction in the circulation aids the cold outflow from the Arctic Ocean through Nares Strait and across northwestern Baffin Bay. Our ocean model experiment suggests that the AOW layer propagating up the west coast of Greenland has warmed by at least a factor of two since at least 2001, and its associated heat transfer has impacted ice growth across northern Baffin Bay. Previous studies have suggested that AOW warming in the WGC began in the mid-to-late

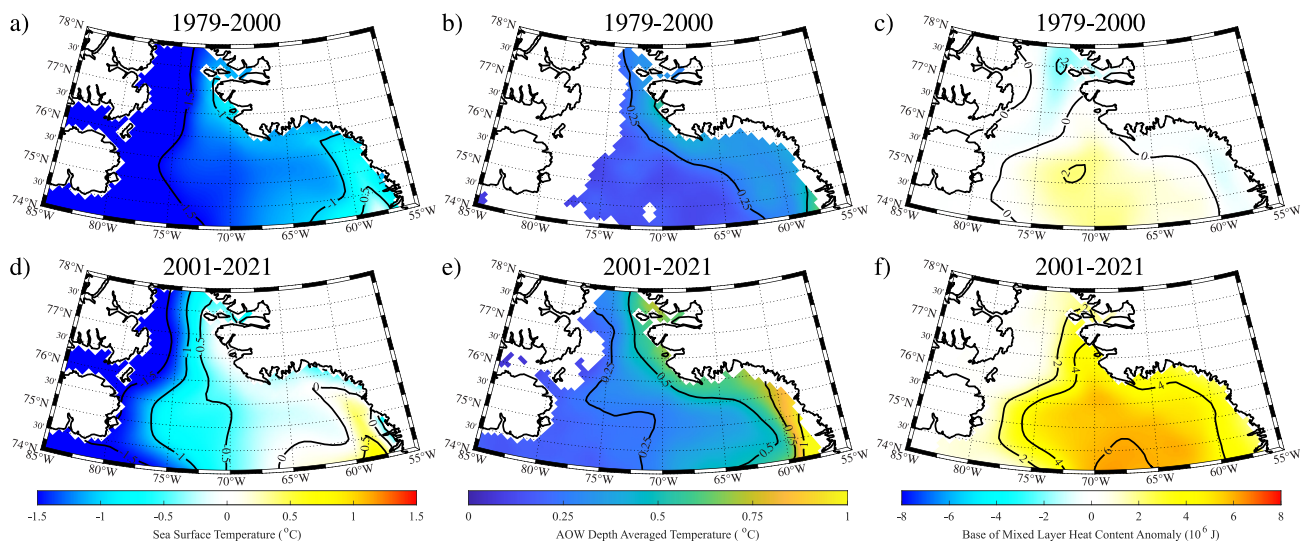


Figure 5. The changing nature of oceanic conditions in northern Baffin Bay during October 1979–2021. For the period 1979–2000: (a) sea surface temperature (°C), (b) depth-averaged temperature of Atlantic-origin water (°C), and (c) base of mixed layer heat content anomaly relative to 1979 (10^6 J). The same fields, but for 2001–2021, are shown in (d), (e), and (f). All data are from the NEMO model run.

1990s, accelerating west Greenland outlet glacier melt (Myers & Ribergaard, 2013; Wood et al., 2021) and delaying widespread freeze-up of Baffin Bay (Ballinger et al., 2018). Longer periods of above-freezing upper-ocean conditions in Baffin Bay during autumn have implications for lengthening the GrIS melt season, particularly for marine-terminating glaciers (Ballinger et al., 2021).

Multiple factors likely contribute to Baffin Bay and broader AOW warming, such as coupled processes associated with Atlantic multidecadal variability, its warming, and overlying atmospheric pressure patterns (Hanna et al., 2013; Lapointe et al., 2020). The main North Atlantic climate modes, including NAO, GBI, and AMO, exhibit some variability since 2001 (Figure S5 in Supporting Information S1). However, Pettitt changepoints within each of these indices signal a mean or variance shift leading the Baffin Bay SIA changes by 6–13 years. Lagged ocean-atmosphere interactions including intraseasonal processes (e.g., the local ice-albedo feedback; Stroeve et al., 2016) and interannual variability (e.g., tropical SST teleconnections with the high-latitude atmosphere; Ding et al., 2014) may also play a key role in Baffin Bay's warming and ice loss and are the subject of ongoing investigations.

Data Availability Statement

ERA5 data are available from <https://cds.climate.copernicus.eu/cdsapp%23%21/dataset/reanalysis%2Dera5%2Dpressure%2Dlevels%3Ftab%3Doverview>, DMI data are available from <https://www.dmi.dk/publikationer/>, and the CDR product, the primary sea-ice dataset analyzed, is available from NSIDC at <https://nsidc.org/data/g02202>. The SIBT1850 data are available from <https://nsidc.org/data/g10010/versions/2>.

Acknowledgments

The authors thank John Cappelen and Caroline Drost Jensen for their assistance obtaining the Kitsissut weather station data and Baojuan Huai for sharing the Pettitt's test via a Matlab script. The authors thank the editor and two reviewers for their remarks, which led to an improved manuscript.

References

- Ballinger, T. J., Hanna, E., Hall, R. J., Carr, J. R., Brasher, S., Osterberg, E. C., et al. (2021). The role of blocking circulation and emerging open water feedbacks on Greenland cold-season air temperature variability over the last century. *International Journal of Climatology*, *41*, E2778–E2800. <https://doi.org/10.1002/joc.6879>
- Ballinger, T. J., Hanna, E., Hall, R. J., Miller, J., Ribergaard, M. H., & Høyer, J. L. (2018). Greenland coastal air temperatures linked to Baffin Bay and Greenland Sea ice conditions during autumn through regional blocking patterns. *Climate Dynamics*, *50*, 83–100. <https://doi.org/10.1007/s00382-017-3583-3>
- Bamber, J. L., Westaway, R. M., Marzeion, B., & Wouters, B. (2018). The land ice contribution to sea level during the satellite era. *Environmental Research Letters*, *13*, 063008. <https://doi.org/10.1088/1748-9326/aac2f0>
- Barber, D. G., Hanesiak, J. M., Chan, W., & Piwowar, J. (2001). Sea-ice and meteorological conditions in Northern Baffin Bay and the North Water polynya between 1979 and 1996. *Atmosphere-Ocean*, *39*, 343–359. <https://doi.org/10.1080/07055900.2001.9649685>
- Cappelen, J. (Ed.) (2021). *Weather observations from Greenland 1958–2000. DMI Report 21-08*. Danish Meteorological Institute. Retrieved from <https://www.dmi.dk/publikationer/>

- Castro de la Guardia, L., Garcia-Quintana, Y., Claret, M., Hu, X., Galbraith, E. D., & Myers, P. G. (2019). Assessing the Role of High-Frequency Winds and Sea Ice Loss on Arctic Phytoplankton Blooms in an Ice-Ocean-Biogeochemical Model. *Journal of Geophysical Research: Biogeosciences*, *124*, 2728–2750. <https://doi.org/10.1029/2018JG004869>
- Castro de la Guardia, L., Hu, X., & Myers, P. G. (2015). Potential positive feedback between Greenland Ice Sheet melt and Baffin Bay heat content on the west Greenland shelf. *Geophysical Research Letters*, *42*, 4922–4930. <https://doi.org/10.1002/2015GL064626>
- Cooley, S. W., Ryan, J. C., Smith, L. C., Horvat, C., Pearson, B., Dale, B., & Lynch, A. H. (2020). Coldest Canadian Arctic communities face greatest reductions in shorefast sea ice. *Nature Climate Change*, *10*, 533–538. <https://doi.org/10.1038/s41558-020-0757-5>
- Ding, Q., Wallace, J. M., Battisti, D. S., Steig, E. J., Gallant, A. J. E., Kim, H.-J., & Geng, L. (2014). Tropical forcing of the recent rapid Arctic warming in northeastern Canada and Greenland. *Nature*, *509*, 209–212. <https://doi.org/10.1038/nature13260>
- Dunbar, M. (1969). The geographical position of the North Water. *Arctic*, *22*, 438–441. <https://doi.org/10.14430/arctic3235>
- Egbert, G. D., & Erofeeva, S. Y. (2002). Efficient Inverse Modeling of Barotropic Ocean Tides. *Journal of Atmospheric and Oceanic Technology*, *19*, 183–204. [https://doi.org/10.1175/1520-0426\(2002\)019<0183:eimob>2.0.co;2](https://doi.org/10.1175/1520-0426(2002)019<0183:eimob>2.0.co;2)
- Grumet, N. S., Wake, C. P., Mayewski, P. A., Zielinski, G. A., Whitlow, S. I., Koerner, R. M., et al. (2001). Variability of sea-ice extent in Baffin Bay over the Last Millennium. *Climate Change*, *49*, 129–145. <https://doi.org/10.1023/A:1010794528219>
- Hanna, E., Jones, J., Cappelen, J., Mernild, S. H., Wood, L., Steffen, K., & Huybrechts, P. (2013). The influence of North Atlantic atmospheric and oceanic forcing effects on 1900–2010 Greenland summer climate and ice melt/runoff. *International Journal of Climatology*, *33*, 862–880. <https://doi.org/10.1002/joc.3475>
- Heinemann, G. (2003). Forcing and feedback mechanisms between katabatic wind and sea ice in the coastal areas of polar ice sheets. *Journal of Atmospheric and Oceanic Science*, *4*, 169–201. <https://doi.org/10.1080/1023673042000198130>
- Hersbach, H., Bell, B., Berrisford, P., Hirahara, S., Horányi, A., Muñoz-Sabater, J., et al. (2020). The ERA5 Global Reanalysis. *Quarterly Journal of the Royal Meteorological Society*, *146*, 1999–2049. <https://doi.org/10.1002/qj.3803>
- Hu, X., Sun, J., Chan, T. O., & Myers, P. G. (2018). Thermodynamic and dynamic ice thickness contributions in the Canadian Arctic Archipelago in NEMO-LIM2 numerical simulations. *The Cryosphere*, *12*, 1233–1247. <https://doi.org/10.5194/tc-12-1233-2018>
- Ingram, R. G., Bâcle, J., Barber, D. G., Gratton, Y., & Melling, H. (2002). An overview of physical processes in the North Water. *Deep-Sea Research Part II*, *49*, 4893–4906. [https://doi.org/10.1016/S0967-0645\(02\)00169-8](https://doi.org/10.1016/S0967-0645(02)00169-8)
- Kalnay, E., Kanamitsu, M., Kistler, R., Collins, W., Deaven, D., Gandin, L., et al. (1996). The NCEP/NCAR 40-year reanalysis project. *Bulletin of the American Meteorological Society*, *77*, 437–471. [https://doi.org/10.1175/1520-0477\(1996\)077<0437:tnypr>2.0.co;2](https://doi.org/10.1175/1520-0477(1996)077<0437:tnypr>2.0.co;2)
- Lapointe, F., Bradley, R. S., Francus, P., Balascio, N. L., Abbott, M. B., Stoner, J. S., et al. (2020). Annually resolved Atlantic sea surface temperature variability over the past 2,900 y. *Proceedings of the National Academy of Sciences*, *117*, 27171–27178. <https://doi.org/10.1073/pnas.2014166117>
- Large, W. G., & Yeager, S. G. (2008). The global climatology of an interannually varying air–sea flux data set. *Climate Dynamics*, *33*, 341–364. <https://doi.org/10.1007/s00382-008-0441-3>
- Madec, G., Bourdallé-Badie, R., Chanut, J., Clementi, E., Coward, A., Ethé, C., et al. (2008). *NEMO ocean engine*. Notes Du Pôle de Modélisation, Institut Pierre-Simon Laplace (IPSL), France.
- Meier, W. N., Fetterer, F., Windnagel, A. K., & Stewart, J. S. (2021). *NOAA/NSIDC Climate Data Record of Passive Microwave Sea Ice Concentration, Version 4*. NSIDC: National Snow and Ice Data Center. <https://doi.org/10.7265/efmz-2665>
- Meier, W. N., Stewart, J. S., Windnagel, A., & Fetterer, F. M. (2022). Comparison of hemispheric and regional sea ice extent and area trends from NOAA and NASA passive microwave-derived climate records. *Remote Sensing*, *14*, 619. <https://doi.org/10.3390/rs14030619>
- Meier, W. N., Stroeve, J., & Gearhead, S. (2006). Bridging perspectives from remote sensing and Inuit communities on changing sea-ice cover in the Baffin Bay region. *Annals of Glaciology*, *44*, 433–438. <https://doi.org/10.3189/172756406781811790>
- Melling, H., Gratton, Y., & Ingram, G. (2001). Ocean circulation within the North Water polynya of Baffin Bay. *Atmosphere-Ocean*, *39*, 301–325. <https://doi.org/10.1080/07055900.2001.9649683>
- Moon, T., Joughin, I., & Smith, B. (2015). Seasonal to multiyear variability of glacier surface velocity, terminus position, and sea ice/ice mélange in northwest Greenland. *J. Geophys. Res. Earth Surface*, *120*, 818–833. <https://doi.org/10.1002/2015JF003494>
- Moore, G. W. K. (2006). Reduction in seasonal sea ice concentration surrounding southern Baffin Island 1979–2004. *Geophysical Research Letters*, *33*, L20501. <https://doi.org/10.1029/2006GL027764>
- Moore, G. W. K., Howell, S. E. L., Brady, M., Xu, X., & McNeil, K. (2021). Anomalous collapses of Nares Strait ice arches leads to enhanced export of Arctic sea ice. *Nature Communications*, *12*. <https://doi.org/10.1038/s41467-020-20314-w>
- Myers, P. G., & Ribergaard, M. H. (2013). Warming of the Polar Water Layer in Disko Bay and potential impact on Jakobshavn Isbrae. *Journal of Physical Oceanography*, *43*, 2629–2640. <https://doi.org/10.1175/JPO-D-12-051.1>
- Onarheim, I. H., Eldevik, T., Smedsrud, L. H., & Stroeve, J. C. (2018). Seasonal and regional manifestation of Arctic sea ice loss. *Journal of Climate*, *31*, 4917–4932. <https://doi.org/10.1175/JCLI-D-17-0427.1>
- Pettitt, A. N. (1979). A non-parametric approach to the change-point problem. *Journal of the Royal Statistical Society: Ser. C*, *28*, 126–135. <https://doi.org/10.2307/2346729>
- Selleveid, R., Lenaerts, J. T. M., & Vizcaino, M. (2022). Influence of Arctic sea-ice loss on the Greenland ice sheet climate. *Climate Dynamics*, *58*, 179–193. <https://doi.org/10.1007/s00382-021-05897-4>
- Stadnyk, T. A., MacDonald, M. K., Tefs, A., Déry, S. J., Koenig, K., Gustafsson, D., et al. (2020). Hydrological modeling of freshwater discharge into Hudson Bay using HYPE. *Elementa: Science of the Anthropocene*, *8*. <https://doi.org/10.1525/elementa.439>
- Stern, H. L., & Heide-Jørgensen, M. P. (2003). Trends and variability of sea ice in Baffin Bay and Davis Strait, 1953–2001. *Polar Research*, *22*, 11–18. <https://doi.org/10.3402/polar.v22i1.6438>
- Stroeve, J., & Notz, D. (2018). Changing state of Arctic sea ice across all seasons. *Environmental Research Letters*, *13*, 103001. <https://doi.org/10.1088/1748-9326/aade56>
- Stroeve, J. C., Crawford, A. D., & Stammerjohn, S. (2016). Using timing of ice retreat to predict timing of fall freeze-up in the Arctic. *Geophysical Research Letters*, *43*, 6332–6340. <https://doi.org/10.1002/2016GL069314>
- Stroeve, J. C., Mioduszewski, J. R., Rennermalm, A., Boisvert, L. N., Tedesco, M., & Robinson, D. (2017). Investigating the local-scale influence of sea ice on Greenland surface melt. *The Cryosphere*, *11*, 2363–2381. <https://doi.org/10.5194/tc-11-2363-2017>
- Titchner, H. A., & Rayner, N. A. (2014). The Met Office Hadley Centre sea ice and sea surface temperature data set, version 2: 1. Sea ice concentrations. *Journal of Geophysical Research: Atmospheres*, *119*, 2864–2889. <https://doi.org/10.1002/2013JD020316>
- Vancoppenolle, M., Fichet, T., Goosse, H., Bouillon, S., Madec, G., & Maqueda, M. A. M. (2009). Simulating the mass balance and salinity of Arctic and Antarctic sea ice. 1. Model description and validation. *Ocean Modelling*, *27*, 33–53. <https://doi.org/10.1016/j.ocemod.2008.10.005>
- Walsh, J. E., Chapman, W. L., Fetterer, F., & Stewart, J. S. (2019). *Gridded monthly sea ice extent and concentration, 1850 onward, version 2*. National Snow and Ice Data Center. <https://doi.org/10.7265/jj4s-tq79>

Wood, M., Rignot, E., Fenty, I., An, L., Björk, A., Broeke, M., et al. (2021). Ocean forcing drives glacier retreat in Greenland. *Science Advances*, 7, 1–10. <https://doi.org/10.1126/sciadv.aba7282>

References From the Supporting Information

- Brennan, M. K., Hakim, G. J., & Blanchard-Wrigglesworth, E. (2020). Arctic sea-ice variability during the instrumental era. *Geophysical Research Letters*, 47, e2019GL086843. <https://doi.org/10.1029/2019GL086843>
- Cavalieri, D. J., Gloersen, P., & Campbell, W. J. (1984). Determination of sea ice parameters with the NIMBUS 7 SMMR. *Journal of Geophysical Research*, 89, 5355–5369. <https://doi.org/10.1029/JD089iD04p05355>
- Cavalieri, D. J., Parkinson, C. L., Gloersen, P., & Zwally, H. J. (1996). Sea Ice Concentrations from Nimbus-7 SMMR and DMSP SSM/I-SSMIS Passive Microwave Data, Version 1. Boulder, Colorado USA. NASA National Snow and Ice Data Center Distributed Active Archive Center. <https://doi.org/10.5067/8GQ8LZQVL0VL>
- Comiso, J. C. (1986). Characteristics of winter sea ice from satellite multispectral microwave observations. *Journal of Geophysical Research*, 91, 975–994. <https://doi.org/10.1029/JC091iC01p00975>
- Comiso, J. C. (2017). Bootstrap Sea Ice Concentrations from Nimbus-7 SMMR and DMSP SSM/I-SSMIS, Version 3. Boulder, Colorado USA. NASA National Snow and Ice Data Center Distributed Active Archive Center. <https://doi.org/10.5067/7Q8HCCWS410R>
- Fetterer, F., Knowles, K., Meier, W. N., Savoie, M., & Windnagel, A. K. (2017). *Updated daily: Sea Ice Index, Version 3.0*. NSIDC: National Snow and Ice Data Center. <https://doi.org/10.7265/N5K072F8>
- Renfrew, I. A., Barrell, C., Elvidge, A. D., Brooke, J. K., Duscha, C., King, J. C., et al. (2020). An evaluation of surface meteorology and fluxes over the Iceland Greenland Seas in ERA5 reanalysis: The impact of sea ice distribution. *Quarterly Journal of the Royal Meteorological Society*, 147, 691–712. <https://doi.org/10.1002/qj.3941>